COORDINATED ELECTRIC VEHICLE CHARGING – PERFORMANCE ANALYSIS OF DEVELOPED ALGORITHMS

Daniel-Leon Schultis [1*], Alfred Einfalt [2], Paul Zehetbauer [3], Daniel Herbst [4]

[1]TU Wien, ESEA, Gußhausstraße 25/370-01, Vienna, Austria
[2]Siemens AG Oesterreich, Siemensstrasse 90, Vienna, Austria
[3]AIT Austrian Institute of Technology GmbH, Giefinggasse 4, Vienna, Austria
[4]Graz University of Technology, IEAN, Inffeldgasse 18/I, Graz, Austria
**daniel-leon.schultis@tuwien.ac.at*

Keywords: LOW VOLTAGE GRID, ELECTRIC VEHICLE CHARGING STATION, SMART GRID, CONGESTION MANAGEMENT, PHOTOVOLTAIC.

Abstract

The increasing use of electric vehicle charging stations with high simultaneity may provoke overloading of low voltage grids. These congestions can be managed by using algorithms that coordinate the distributed charging processes. This study includes a load flow-based performance analysis of three coordination algorithms that allow for charging with either minimal or maximal power. The algorithms differ in the number of control signals they specify: the use of one global control signal, one control signal per feeder, and one control signal per charging station is considered. The performance of each algorithm is analysed for complete and rudimentary knowledge of the photovoltaic production and the consumption of household appliances. Results show that all algorithms effectively mitigate transformer and line segment overloading. The more individual control signals are specified, the lower is the resulting average charging time, and the higher is the energy loss. In the analysed scenario, the lack of knowledge concerning the power contributions of photovoltaic systems and household appliances does not significantly impair the performance of the algorithms.

1 Introduction

The number of photovoltaic (PV) systems and electric vehicle charging stations (EVCS) located in residential customer plants (CP) rapidly increases. Simultaneous electric vehicle (EV) charging directly after rush hour may provoke overloading of the distribution transformer (DTR) and line segments in low voltage (LV) level. Meanwhile, the distributed PV injections aggravate the overload detection based on the power flows in distribution substation. Grid reinforcement effectively mitigates the congestions during peak load periods, but leads to relatively poor asset utilization in the remaining time. Smart grids intend to increase the asset utilization by employing power system operation processes such as monitoring and congestion management, which are traditionally conducted only in (sub-) transmission grids, also in distribution level. In this context, congestion management by coordinated EV charging becomes an alternative to grid reinforcement. Therefore, the power absorbed by the EVCSs may be adapted continuously or in discrete steps, whereby the simplest approach is to allow for charging with either maximal or minimal power. On this basis, the presented study, which is part of the Austrian flagship project 'PoSyCo' [1], analyses the performance of three coordination algorithms that specify either one control signal per LV grid, one per LV feeder, or one per EVCS.

$U_{i,t}$	Supply voltage of CP *i* at *t*
$P_{i,t}^{Dev}$, $Q_{i,t}^{Dev}$	Dev-model power contributions of CP *i* at *t*
$P_{nom,i,t}^{Dev}$ $Q_{nom,i,t}^{Dev}$	Dev-model power contributions of CP *i* at *t* for nominal supply voltage
$P_{i,t}^{Pr}$, $Q_{i,t}^{Pr}$	Pr-model power contributions of CP *i* at *t*
P_{max}^{Pr}, Q_{max}^{Pr}	Maximal Pr-model power contributions
$P_{i,t}^{St}$ $P_{nom,i,t}^{St}$	St-model active power contribution for actual and nominal supply voltage of CP *i* at *t*
P_{max}^{St}, P_{min}^{St}	Max. and min. St-model charging power
$SoC_{i,t}^{St}$	St-model state-of-charge of CP *i* at *t*
E_{max}^{St}	St-model storage capacity
Δt	Resolution of load profiles
U_{prim}^{DTR}	Voltage at DTR primary bus bar

2 Methodology

The developed coordination algorithms are analysed using load flow simulations in a combined LV grid and CP model. The model is implemented, and the load flow (LF) calculations are conducted in PSS SINCAL, while the algorithms are implemented in MATLAB. Both tools are connected through the COM-interface.

2.1 Model description

The scope of this study is set on LV and CP level. Therefore, both levels are included in the used power system model.

2.1.1 Low voltage grid: Figure 1a shows the simplified one-line diagram of the LV grid model. It represents a real urban grid with a cable share of 81 % that connects 91 residential CPs. The 20 kV / 0.4 kV distribution transformer is rated with 630 kVA and has its tap changer fixed in mid-position. The slack node is located at the DTR primary bus bar.

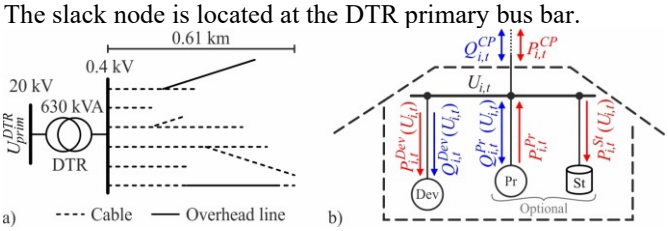

Fig. 1 Power system model: (a) Simplified one-line diagram of the low voltage grid, (b) Structure of the customer plant.

2.1.2 Customer plant: Figure 1b shows the structure of the CP model. It includes three components: the device (Dev), producer (Pr), and storage (St) model, representing the household appliances, the PV system, and the EV battery, respectively. The latter ones are optional as the PV and EVCS penetrations are set to approximately 50 %, i.e. 46 CPs include a PV system and an EVCS. Asymmetry is not considered. The Dev-model power contributions depend on the CP supply voltage, Eq. (1). Therein, ZIP-coefficients from [2] are used; and power contributions at nominal voltage are defined by load profiles.

$$P_{i,t}^{Dev} = P_{nom,i,t}^{Dev} \cdot \left(1.31 \cdot U_{i,t}^2 - 1.94 \cdot U_{i,t} + 1.63\right) \quad (1a)$$

$$Q_{i,t}^{Dev} = Q_{nom,i,t}^{Dev} \cdot \left(9.2 \cdot U_{i,t}^2 - 15.27 \cdot U_{i,t} + 7.07\right) \quad (1b)$$

The voltage-independent active power injections of the Pr-models are defined by one common load profile. Meanwhile, their reactive power contributions are determined by the common $Q(U)$-characteristic suggested as default in [3]. The maximum reactive power value is set according to Eq. (2).

$$Q_{max}^{Pr} = 0.4843 \cdot P_{max}^{Pr} \quad (2a)$$

$$P_{max}^{Pr} = 5\ \text{kW} \quad (2b)$$

The voltage-dependent St-model's active power consumption is determined by Eq. (3a); ZIP-coefficients from [4] are used. The corresponding reactive power contributions are set to zero. Eq. (3b) is used to calculate the actual state-of-charge (SoC).

$$P_{i,t}^{St} = P_{nom,i,t}^{St} \cdot \left(-0.02 \cdot U_{i,t}^2 + 0.03 \cdot U_{i,t} + 0.99\right) \quad (3a)$$

$$SoC_{i,t}^{St} = SoC_{i,t-1}^{St} + \Delta t \cdot P_{i,t-1}^{St} / E_{max}^{St} \quad (3b)$$

The batteries are charged whenever condition (4) is satisfied.

$$SoC_{i,t}^{St} < 99\ \% \quad \text{and} \quad t \geq t_{start,i}^{St} \quad (4)$$

When charging, Eq. (5) determines the corresponding active power consumption at nominal voltage, and otherwise, it is set to zero.

$$P_{nom,i,t}^{St} = P_{max}^{St} \quad \text{When permission granted} \quad (5a)$$

$$P_{nom,i,t}^{St} = P_{min}^{St} \quad \text{When permission denied} \quad (5b)$$

2.2 Scenario definition

Figures 2a and b show the load profiles of the Dev- and Pr-models, created with the tool described in [5]. For the Dev-model of each CP are used individual profiles. The reactive power profile is derived from the active power one using an inductive power factor of 0.95. Due to the spatial proximity of all CPs connected to one LV grid, the same load profile is used for all Pr-models. This profile is characterised by spikes that are provoked by clouds. In each CP, the charging process is initiated at an individual instant of time, defined according to a normal distribution with mean value μ = 18:00 and the standard deviation σ = 1 h. The selected mean value corresponds to the daytime at which most working residents arrive at their homes [6]. Initially, the SoC of each EV battery is set to 25 %. The corresponding storage capacity, and the maximal and minimal charging power are set to 40 kWh, 11 kW and 5 kW, respectively. The DTR primary voltage of 1.00 p.u. is used.

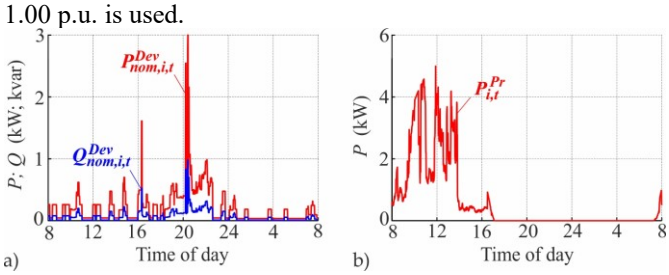

Fig. 2 Actual load profiles of different CP components: (a) Dev-model, (b) Pr-model.

2.3 Charge requests

Whenever condition (4) is satisfied, the algorithm executing device receives charge requests from the corresponding EVCSs. As long as no permissions are granted, they charge with the minimal power.

2.4 Grid state calculations

The decisions of the coordination algorithms rely on estimations of the LV grid state. State estimation (SE) in LV level is a complex topic, which is out of the scope of this study. Instead of implementing a real SE algorithm coping with measurement errors, bad data, etc., the grid state is estimated by calculating the LF in the deposited power system model for assumed DTR primary voltage and load behaviour. To analyse the coordination algorithms and the impact of the knowledge of the load behaviour separately, two cases are considered: complete and rudimentary knowledge of load behaviour.

2.4.1 Complete load knowledge: The LF is calculated using the ideal power system model including the actual ZIP-coefficients and $Q(U)$-characteristic of the CP model components; and the actual load profiles and DTR primary voltage, Eq. (6).

$$\tilde{U}_{prim}^{DTR} = U_{prim}^{DTR} \quad (6a)$$

$$\tilde{P}_{nom,i,t}^{Dev} = P_{nom,i,t}^{Dev} \qquad \tilde{Q}_{nom,i,t}^{Dev} = Q_{nom,i,t}^{Dev} \quad (6b)$$

$$\tilde{P}_{i,t}^{Pr} = P_{i,t}^{Pr} \quad (6c)$$

Where the accent "~" indicates the values used for state calculation.

2.4.2 Rudimentary load knowledge: The ideal grid model but incomplete CP model parameters are available for the LF

calculations. While the exact $Q(U)$-characteristic is known, the ZIP-coefficients are unknown; constant power models are employed instead of using Eq. (1) and (3a). The exact DTR primary voltage and estimated load profiles are used. For all Dev-models the standard load profile [7] shown in Fig. 3a is used. The profile is scaled so as to reach the same maximum value as the mean of the actual Dev-model active power consumptions. The appearance of clouds and thus the spikes on the load profile of PV-systems can hardly be forecasted. Therefore, the profile resulting from the clear sky radiation is used as an estimation of the Pr-model active power injections, Fig. 3b.

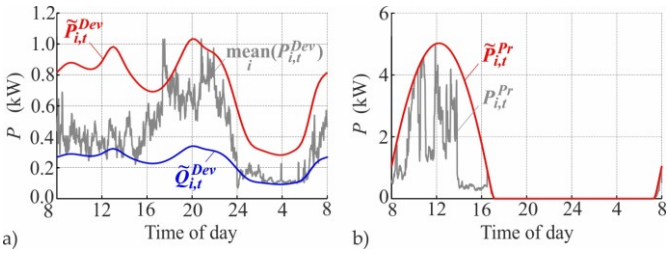

Fig. 3 Estimated load profiles of different CP components: (a) Dev-model, (b) Pr-model.

3 Coordination algorithms

The analysed coordination algorithms rely on the generalized flow chart shown in Fig. 4. As the algorithms reduce the power consumption of EVCSs when potential congestions are detected, they can only mitigate loading limit violations provoked by downstream active power flows, i.e., from DTR to LV feeder end, in fact regardless of the reactive power flow directions. When starting the algorithms, all charge requests are initially permitted. To prepare the LF calculations, the active power contributions of the St-models are specified according Eq. (7) and the present permissions; and the reactive ones are set to zero.

$$\tilde{P}_{i,t}^{St} = P_{max}^{St} \quad \text{When request is presently permitted} \quad (7a)$$

$$\tilde{P}_{i,t}^{St} = P_{min}^{St} \quad \text{When request is presently denied} \quad (7b)$$

$$\tilde{P}_{i,t}^{St} = 0 \quad \text{Without request from CP } i \text{ at } t \quad (7c)$$

Meanwhile, the power contributions of the Dev- and Pr-models are set for complete and rudimentary load knowledge according to the actual and estimated load profiles and DTR primary voltage, respectively, as described in section 2.4. Subsequently, the LF engine uses the LV and CP models to calculate the grid state that would result from the present permissions. If violations of the configured line segment loading limits are detected, the permissions of selected EVCS are denied, and the preparation and execution of LF is repeated. This cycle is repeated until no violations of the line segment loading limits remain, or all permissions are denied. In the latter case, the algorithms are not sufficient to eliminate all limit violations, and total charging prohibition should be considered. When no limit violations occur in the feeders, the actual LF results are examined for violations of the configured DTR loading limit. If limit violations are detected and permissions are still active, the permissions of selected EVCSs are denied and the LF preparation and execution are repeated. Otherwise, the control signals are sent to the EVCSs. Different options may be used for the selection processes of EVCSs for permission denial, i.e. for the process-steps represented by the two coloured boxes in Fig. 4. Three options are investigated: one control signal per LV grid, one per LV feeder, and one per EVCS.

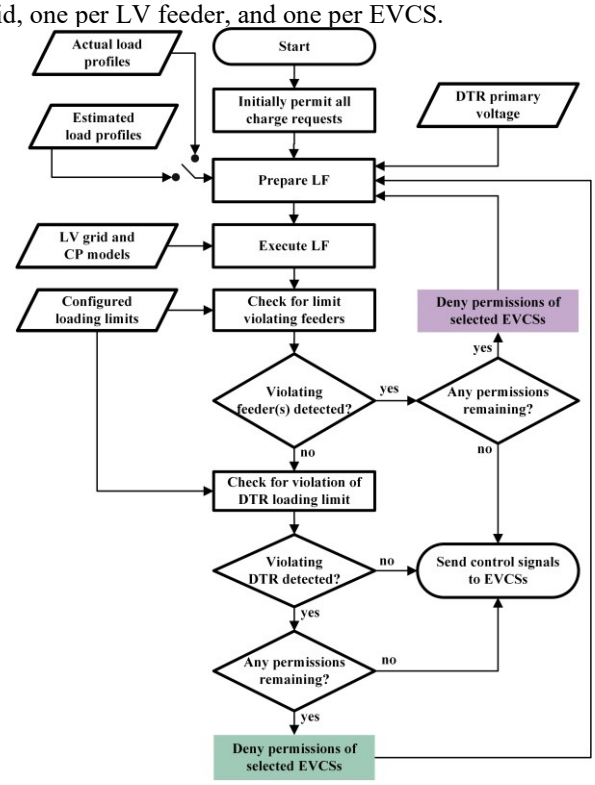

Fig. 4 Generalized flow chart of the coordination algorithms.

3.1 One control signal per LV grid

The same control signal is sent to all EVCSs connected to the LV grid. When limit violations in line segments or the DTR are detected, the permissions of all EVCSs are denied (both coloured boxes).

3.2 One control signal per LV feeder

The same control signal is sent to all EVCSs connected to one LV feeder. When a limit violating feeder is detected, the permissions of all thereto connected EVCSs are denied (violet box). When no feeder but the DTR violates its limit, all EVCSs connected to one random feeder are selected for permission denial (green box).

3.3 One control signal per EVCS

An individual control signal is sent to each EVCS. When a limit violating feeder is detected, the permission of one random EVCS connected behind the most distant (from DTR) violating line segment is denied (violet box), Fig. 5. When no feeder but the DTR violates its limit, one random EVCS is selected for permission denial (green box).

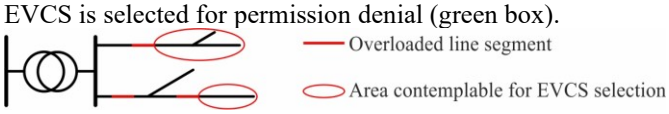

Fig. 5 Selection of EVCS for one control signal per EVCS.

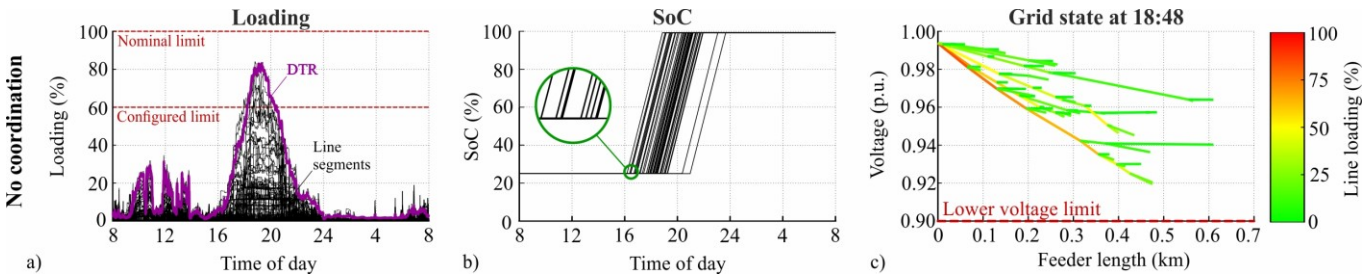

Fig. 6 Simulation results without coordination: (a) Asset loading, (b) SoC of all EV batteries, (c) Grid state at 18:50.

4 Performance of coordination algorithms

The execution period of the algorithms is set to five minutes, i.e. the algorithms are executed each 5th minute. It is assumed that the resulting control signals are available at the EVCSs in the next simulated instant of time, i.e. by no later than one minute. The configured loading limits of the DTR and line segments are set to 60 %. Table 1 summarizes the total energy loss of the DTR and all line segments, and the average charging time per EV for all simulated coordination setups. Figure 6 shows the simulation results without coordination. As Fig. 6a illustrates, violations of the configured loading limits appear between 17:56 and 20:26. The EV batteries are charged between 16:10 and 23:40, Fig. 6b. The charging with maximal power provokes linear increases of the battery SoCs, an average charging time of 161.00 min, and energy losses of 64.32 kWh. The grid state at 18:48, where the maximal loading value appears, is shown in Fig. 6c. The line segment loading decreases from substation to feeder end, reaching its highest values in the foremost line segments. The lower voltage limit is not violated. Figure 7 shows the simulation results for the coordination setups with complete knowledge of the load behaviour. If one control signal per LV grid is used, two line segments slightly violate the configured limit at 17:58, Fig. 7a. The EVCSs start charging with minimal power and change to the maximal one as soon as the permissions are received, i.e. after maximum 4 minutes (due to the selected execution period of 5 min). All permissions are denied between 17:59 and 23:24, increasing the average charging time to 305.39 min, and decreasing the energy loss to 45.17 kWh.

Table 1 Energy loss and average charging time per EV for all simulated coordination setups.

Knowledge of load behaviour	Control signals	Energy loss (kWh)	Average charging time per EV (min)
-	None	64.32	161.00
Complete	One per LV grid	45.17	305.39
	One per LV feeder	53.53	222.63
	One per EVCS	56.60	196.11
Rudimentary	One per LV grid	44.19	312.11
	One per LV feeder	53.00	226.74
	One per EVCS	54.39	211.59

In Fig. 7b, temporary violations of the configured loading limits appear. The feeder-wise permission denial provokes an average charging time of 222.63 min, and an energy loss of 53.53 kWh. When individual control signals are used for each

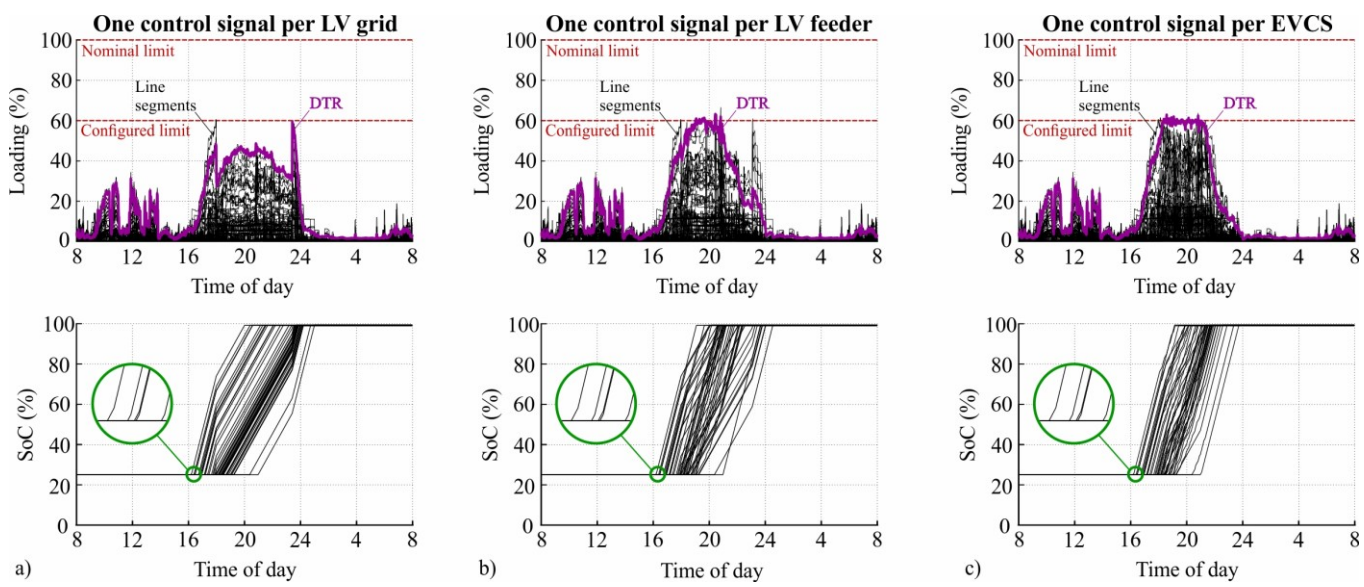

Fig. 7 Asset loading and SoC of all EV batteries for complete knowledge of the load behaviour and different coordination algorithms: (a) One control signal per LV grid, (b) One control signal per LV feeder, (c) One control signal per EVCS.

EVCS, the maximum loading sticks close to the configured limit, Fig. 7c. The result is an average charging time of 196.11 min and an energy loss of 56.60 kWh. The results of the coordination setups with rudimentary load knowledge are shown in Fig. 8. Here, the global control signal denies permissions between 17:59 and 23:44, i.e. 20 minutes longer as with complete load knowledge, Fig. 8a. This provokes an average charging time of 312.11 min and an energy loss of 44.19 kWh. When one control signal per feeder is used, the configured loading limit is temporarily violated, Fig 8b. With this coordination setup, the charging time averages to 226.74 min, and the losses add up to 53.00 kWh. Regarding the use of individual control signals, Fig. 8c shows that the maximum loading does not stick to the configured limit as close as in the case of complete load knowledge. The average charging time of 211.59 min is reached, provoking an energy loss of 54.39 kWh.

5 Conclusion

The analysed coordination algorithms effectively mitigate distribution transformer and low voltage line segment overloading provoked by electric vehicle charging. The more individual control signals are specified, the lower is the resulting average charging time, and the higher is the grid energy loss. In the analysed scenario, wherein each second customer owns an 11 kW electric vehicle charging station and a 5 kWp photovoltaic system with $Q(U)$-control, the lack of knowledge concerning the photovoltaic production and the consumption of household appliances does not significantly impair the performance of the algorithms. The concern of customer discrimination is not considered in this study. Therefore, further works must develop (e.g. contractual) mechanisms to compensate for the customer discrimination when feeder-wise or individual control signals are used.

6 Acknowledgements

The presented work was funded and supported by the Austrian Research Promotion Agency (FFG) (#867276 PoSyCo) and the Austrian Climate and Energy Fund (KLIEN).

7 References

[1] Einfalt, A., et al., 'Efficient utilisation of existing grid infrastructure empowering smart communities'. Proc. IEEE ISGT, Washington, DC, USA, 2020, pp. 1-5.
[2] Bokhari, A., et al.: 'Experimental Determination of the ZIP Coefficients for Modern Residential, Commercial, and Industrial Loads', IEEE Trans. Power Del., 2014, 29, (3), pp. 1372-1381.
[3] Marggraf, O., et al.: 'U-Control - Analysis of Distributed and Automated Voltage Control in current and future Distribution Grids'. Proc. International ETG Congress, Bonn, Germany, 2017, pp. 1-6.
[4] Shukla, A., Verma, K., and Kumar, R.: 'Multi-stage voltage dependent load modelling of fast charging electric vehicle'. Proc. CERA, Roorkee, 2017, pp. 86-91.
[5] Richardson, I. and Thomson, M.: 'Integrated domestic electricity demand and PV micro-generation model', University of Loughborough (CREST), 2011.
[6] Widhalm, P., Yang, Y., Ulm, M. et al.: 'Discovering urban activity patterns in cell phone data', Transportation, 2015, 42, pp. 597–623.
[7] 'BDEW: Standardlastprofile Strom', https://www.bdew.de/energie/standardlastprofile-strom/, accessed 25 August 2020.

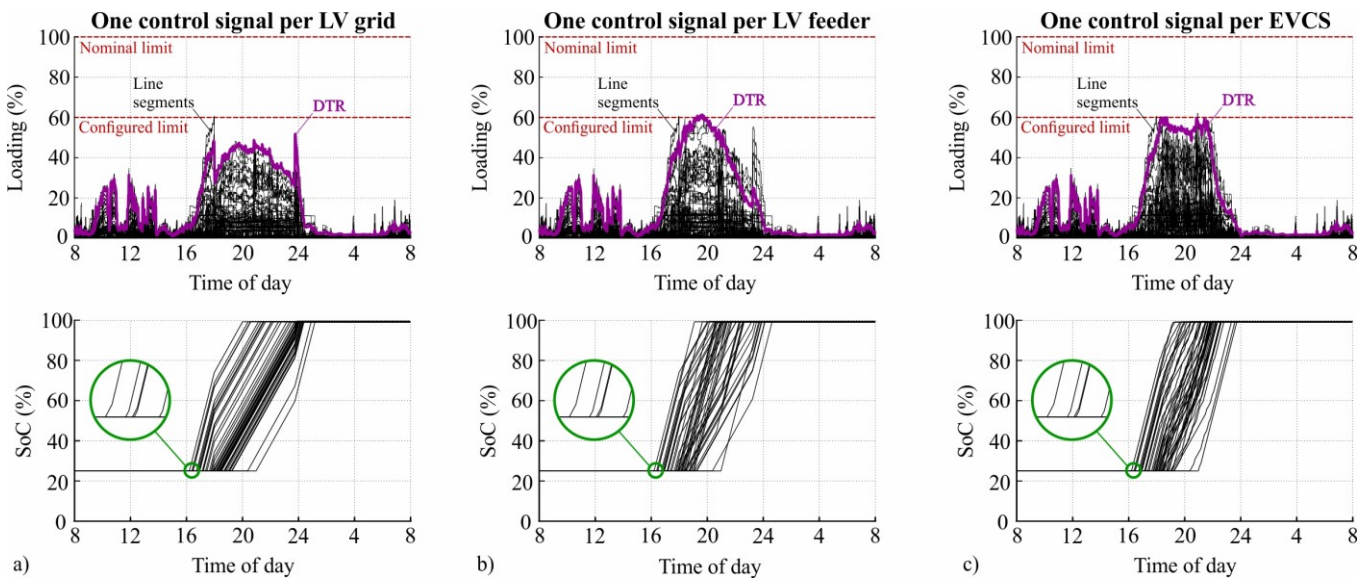

Fig. 8 Asset loading and SoC of all EV batteries for rudimentary knowledge of the load behaviour and different coordination algorithms: (a) One control signal per LV grid, (b) One control signal per LV feeder, (c) One control signal per EVCS.